Investigation of inclined dual-fiber optical tweezers for 3D manipulation and force sensing

Yuxiang Liu and Miao Yu*

Department of Mechanical Engineering, University of Maryland, College Park, MD 20742, USA
**Corresponding author: mmyu@umd.edu*

Abstract: Optical tweezers provide a versatile tool in biological and physical researches. Optical tweezers based on optical fibers are more flexible and ready to be integrated when compared with those based on microscope objectives. In this paper, the three-dimensional (3D) trapping ability of an inclined dual-fiber optical tweezers is demonstrated. The trapping efficiency with respect to displacement is experimentally calibrated along two dimensions. The system is studied numerically using a modified ray-optics model. The spring constants obtained in the experiment are predicted by simulations. It is found both experimentally and numerically that there is a critical value for the fiber inclination angle to retain the 3D trapping ability. The inclined dual-fiber optical tweezers are demonstrated to be more robust to *z*-axis misalignment than the counter-propagating fiber optical tweezers, which is a special case of the former when the fiber inclination angle is 90º. This inclined dual-fiber optical tweezers can serve as both a manipulator and a force sensor in integrated systems, such as microfluidic systems and lab-on-a-chip systems.

OCIS codes: (350.4855) Optical tweezers or optical manipulation; (060.2310) Fiber optics.

References and links

1. K. C. Neuman and S. M. Block, "Optical trapping," Rev. Sci. Instrum. **75**, 2787 (2004).
2. A. Ashkin, "History of optical trapping and manipulation of small-neutral particle, atoms, and molecules," IEEE J. Sel. Top. Quantum Electron. **6**, 841 (2000).
3. D. G. Grier, "Optical tweezers in colloid and interface science," Curr. Opin. Colloid. In. **2**, 264 (1997).
4. S. Hormeno and J. R. Arias-Gonzalez, "Exploring mechanochemical processes in the cell with optical tweezers," Biol. Cell **98**, 679 (2006).
5. E. A. Abbondanzieri, W. J. Greenleaf, J. W. Shaevitz, R. Landick and S. M. Block, "Direct observation of base-pair stepping by RNA polymerase," Nature **438**, 460 (2005).
6. Z. Hu, J. Wang and J. Liang, "Theoretical and experimental investigation of the optical trapping force in single lensed fibre trapping," J. Opt. A-Pure Appl. Op. **8**, 891 (2006).
7. K. Taguchi, H. Ueno, T. Hiramatsu and M. Ikeda, "Optical trapping of dielectric particle and biological cell using optical fibre," Electron. Lett. **33**, 413 (1997).
8. K. S. Abedin, C. Kerbage, A. Fernandez-Nieves and D. A. Weitz, "Optical manipulation and rotation of liquid crystal drops using high-index fiber-optics tweezers," Appl. Phys. Lett. **91**, 091119 (2007).
9. T. Numata, A. Takayanagi, Y. Otani and N. Umeda, "Manipulation of metal nanoparticles using fiber-optic laser tweezers with a microspherical focusing lens," Jpn. J. Appl. Phys. **45**, 359 (2006).
10. R. S. Taylor and C. Hnatovsky, "Particle trapping in 3-D using a single fiber probe with an annular light distribution," Opt. Express, **11**, 2775 (2003), http://www.opticsinfobase.org/oe/abstract.cfm?uri=oe-11-21-2775.
11. Z. Liu, C. Guo, J. Yang and L. Yuan, "Tapered fiber optical tweezers for microscopic particle trapping: fabrication and application," Opt. Express **14,** 12510 (2006), http://www.opticsinfobase.org/oe/abstract.cfm?uri=oe-14-25-12510.
12. L. Yuan, Z. Liu, J. Yang, and C. Guan, "Twin-core fiber optical tweezers," Opt. Express **16**, 4551 (2008), http://www.opticsinfobase.org/oe/abstract.cfm?uri=oe-16-7-4559.
13. C. Liberale, P. Minzioni, F. Bragheri, F. De Angelis, E. Di Fabrizio, and I Cristiani, "Miniaturized all-fiber probe for three-dimensional optical trapping and manipulation," Nat. Photonics **1**, 723 (2007).

#112464 - $15.00 USD Received 10 Jun 2009; revised 10 Jul 2009; accepted 11 Jul 2009; published 23 Jul 2009

14. F. Bragheri, P. Minzioni, C. Liberale, E. Di Fabrizio, and I. Cristiani, "Design and optimization of a reflection-based fiber-optic tweezers," Opt. Express **16**, 17647 (2008), http://www.opticsinfobase.org/oe/abstract.cfm?uri=oe-16-22-17647.
15. M. Wei, K. Yang, A. Karmenyan, and A. Chiou, "Three-dimensional optical force field on a Chinese hamster ovary cell in a fiber-optical dual-beam trap," Opt. Express **14**, 3056 (2006), http://www.opticsinfobase.org/oe/abstract.cfm?uri=oe-14-7-3056.
16. E. Sidick, S. D. Collins, and A. Knoesen, "Trapping forces in a multiple-beam fiber-optic trap," Appl. Optics **36**, 6423 (1997).
17. A. Constable, J. Kim, J. Mervis, F. Zarinetchi and M. Prentiss, "Demonstration of a fiber-optical light-force trap," Opt. Lett. **18**, 1867 (1993).
18. E. R. Lyons and G. J. Sonek, "Confinement and bistability in a tapered hemispheically lensed optical fiber trap," Appl. Phys. Lett. **66**, 1584 (1995).
19. J. Guck, R. Ananthakrishnan, H. Mahmood, T. J. Moon, C. C. Cunningham, J. Kas, "The optical stretcher: a novel laser tool to micromanipulate cells," Biophys. J. **81**, 767 (2001).
20. K. Taguchi, K. Atsuta, T. Nakata and M. Ideda, "Levitation of a microscopic object using plural optical fibers," Opt. Commun. **176**, 43 (2000).
21. K. Taguchi, M. Tanaka and M. Ikeda, "Dual-beam trapping method for an object with large relative refractive index," Jpn. J. Appl. Phys. **39**, L1302 (2000).
22. K. Taguchi, M. Tanaka and M. Ikeda, "Investigation on the radius of a hemispherical microlens of an optical fiber end for three-dimensional trapping," Opt. Quantum Electron. **34**, 993 (2002).
23. S. Vogel, *Life in Moving Fluids: The physical Biology of Flow, Second Edition, Revised and Expanded* (Princeton University Press, 1994), Chap. 15.
24. A. Ashkin, "Forces of a single-beam gradient laser trap on a dielectric sphere in the ray optics regime," Biophys. J. **61**, 569 (1992).
25. H. Lamb, *Hydrodynamics, Sixth Edition* (Dover Publications, 1945), Chapter XI, Page 616.
26. F. Cardarelli, *Materials Handbook, A Concise Desktip Reference, Second Edition* (Springer, 2008), Chap. 10, pp. 672-675.
27. K. Berg-Sørensen and H. Flyvbjerg, "Power spectrum analysis for optical tweezers," Rev. Sci. Instrum. **75**, 594 (2004).
28. R. C. Gauthier, "Optical trapping: a tool to assist optical machining," Opt. Laser Technol. **29**, 389 (1997).
29. Y. Liu and M. Yu, "Three-dimensional fiber optical trap for cell manipulation and force measurement," Proc. SPIE **6528**, 65280Z (2007).
30. A. Priyadarshi, L. H. Fen, S. G. Mhaisalkar, V. Kripesh, and A. K. Asundi, "Fiber misalignment in silicon V-groove based optical modules," Opt. Fiber Technol. **12**, 170 (2006).

1. Introduction

Optical tweezers are widely used in biological and physical researches, [1] such as molecular motors and mechanoenzymes at the single-molecule level, [2] colloidal physics, and mechanical properties of polymers [3]. Optical tweezers can apply forces ranging from tenths to hundreds of picoNewtons to microscale and nanoscale particles [4] and measure displacements with nanometer resolution [1] or even Angstrom resolution [5].

Optical forces arise from the change of photon momentum that the light carries when the light is deflected by a surface. There are two components of the optical forces, the scattering force along the light propagation direction and the gradient force pointing to the highest intensity region. [2] Trapping of microscale particles is enabled by balancing the gradient force with the scattering force and any other forces that the particles are subject to, such as gravities and drag forces. To realize a stable three-dimensional (3D) optical trap with a single beam, a steep intensity gradient, which provides a large gradient force, is necessary. This explains why most of the current optical tweezers are built with microscope objectives [1-5]. An objective with a high numerical aperture (NA) provides a tight focus and hence a large axial optical gradient to achieve 3D trapping ability and a high trapping efficiency. [1, 2]

Optical fibers have also been employed to replace the role of objectives in optical tweezers. [6-22] Since an optical fiber cannot achieve a NA as high as an objective can, fiber optical tweezers usually have lower trapping efficiencies. [6] However, the fiber optical tweezers have irreplaceable advantages over their counterparts based on objectives, such as low cost, flexibility, long working distances, and integratability. Optical forces obtained from

#112464 - $15.00 USD Received 10 Jun 2009; revised 10 Jul 2009; accepted 11 Jul 2009; published 23 Jul 2009

single-fiber optical tweezers (SFOTs) have been investigated both experimentally and theoretically. [6] SFOTs built with lensed fibers can only achieve two-dimensional trapping due to the low NA [6-9]. 3D trapping with SFOTs has been demonstrated by using optical fibers with either a hollow tapered, metalized tip [10] or a tip with an abrupt geometry [11, 12]. The former introduces an electrostatic force to balance the scattering force, and thus it is not purely optical trapping. The latter uses simple fabrication procedure to significantly decrease the spot size of the light emitted from the single-core or twin-core fibers, but the sharp tip results in a focus very close (~ 1 μm) to the fiber end. When the size of a trapped particle is not small enough (e.g., 3 μm), physical contact of the particle is inevitable. Liberale *et al.* [13] proposed a reflection-based optical tweezers with a probe composed of a bundle of four fibers. Bragheri *et al.* [14] later presented the numerical model of this optical tweezers. This setup can achieve 3D trapping and the trap is located ~ 40 μm away from the probe tip. However, when compared with the abovementioned setups, the fabrication procedure is relatively complicated, which requires a focused ion beam (FIB) with the assistance of a scanning electron microscope (SEM). In addition, the orientation of each individual fiber in the fiber bundle needs to be carefully aligned to enable the trap.

A typical arrangement used to achieve 3D trapping is the counter-propagating dual-fiber optical tweezers (DFOTs) built with cleaved (flat-ended) or lensed optical fibers. [15-19] The 3D optical force field obtained from such systems has been investigated both experimentally and numerically. [15, 16] Since fiber alignment is crucial for this arrangement, fibers are generally embedded in a substrate to facilitate the alignment [17-19], which limits the flexibility of fiber optical tweezers. Moreover, due to the relatively large size of the optical fiber, it cannot trap microscale particles lying on the substrate. Taguchi *et al.* [20, 21] developed a DFOTs arrangement with two inclined lensed fibers and demonstrated levitation of microspheres lying on the substrate. The influence of the radius of the fiber tapered end was investigated. [22] The inclined DFOTs provide better flexibility compared with the counter-propagating DFOTs, since the fibers are not necessary to be fixed in substrate. However, this arrangement has not been thoroughly investigated; the trapping efficiency and optical forces along three dimensions have not been studied.

In this paper, the 3D trapping ability of inclined DFOTs is demonstrated. The trapping efficiency of the inclined DFOTs is calibrated experimentally. The calibration enables this setup to be used for force sensing in addition to particle manipulation. The influence of the fiber inclination angle on the trapping performance is studied both experimentally and numerically. The critical inclination angle required to retain a 3D trap is obtained from simulations, which agrees with the experimentally observed value. Numerical simulations of the optical forces along three axes are carried out. In addition to the capability of lifting up particles lying on the substrate, the inclined DFOTs are also found to be more robust to the z-axis misalignment when compared with the counter-propagating DFOTs.

2. Trapping principle of inclined DFOTs

For typical SFOTs built with lensed fiber shown in Fig. 1(a), the trapped particle reaches equilibrium only when there is a normal force N from the substrate. If there is no substrate, the particle will be pushed away. Therefore, SFOTs can only achieve two dimensional (2D) optical trapping.

In the case of the inclined DFOTs as shown in Fig. 1(b), there are two transverse gradient forces (F_{g1} and F_{g2}) and two net axial forces (F_{s1} and F_{s2}) applied by the two beams, respectively. When the four forces are balanced, the particle is three-dimensionally trapped. The equilibrium position is below the intersection of the two beams, and thus, the distance between the trap and the fibers is large enough to manipulate particles of tens of micrometers without any physical contact. It is noted that the gravity and buoyancy are not considered here, whereas in practice to determine whether a 3D trap can be formed, they are important to consider.

#112464 - $15.00 USD Received 10 Jun 2009; revised 10 Jul 2009; accepted 11 Jul 2009; published 23 Jul 2009

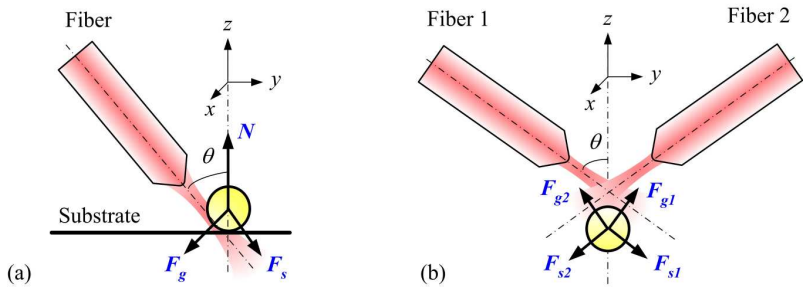

Fig. 1. Illustration of forces applied to a trapped particle in (a) SFOTs and (b) DFOTs. F_s represents the axial net force of the scattering force and the axial gradient force and F_g denotes the transverse gradient force.

A special case of the inclined DFOTs is when the inclination angle of the fibers (θ in Fig. 1(b)) is 90º; i.e., the two fibers are arranged to share the same beam axis, which is known as the counter-propagating DFOTs. In most counter-propagating DFOTs, cleaved fibers are used [19] and the distance between the fiber ends is usually larger than 100 μm. The particle is drawn by the gradient forces to the optical axis where the transverse gradient forces disappear. The scattering forces balance each other to enable a 3D optical trap.

3. Experiment

3.1 Experimental setup

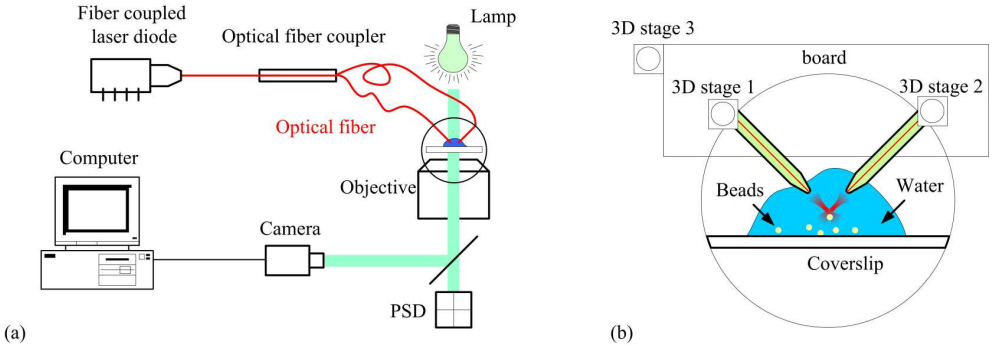

Fig. 2. (a). Experimental setup of the inclined DFOTs system. (b). Close-up showing the optical trap built from the two beams emitted from tapered fibers.

The experimental setup of the inclined DFOTs is shown in Fig. 2(a). An 808 nm laser diode (FMXL808-080SA0B, Bluesky Research) with a maximum power of 70 mW was used as the light source. A 1×2 fiber coupler (Gould Fiber Optics) was employed to split the laser beam into two lensed fibers (OZ Optics). The optical beams exiting from the lensed fibers had Gaussian profiles and formed an optical trap. Each lensed fibers was clamped on a fiber holder so that the suspended fiber length is 10±2 mm. The optical power emitted from the lensed fiber end was measured by using a free-space powermeter (PM144, Thorlabs). All the fibers and the coupler are single-mode at the wavelength of 808 nm. Imaging was realized through a microscope (CKX41, Olympus Inc.) with an oil-immersion objective (PlanC N 100×/1.25, Olympus Inc.). Since the objective is not required to form the optical trap, it can be adjusted freely to visualize different horizontal planes. A CCD camera (Moticam 1000, Motic) was used to capture the videos. For the purpose of calibration, a position-sensitive diode (PSD; DL 100-7PCBA3, Pacific Silicon Sensor Inc.) was utilized to provide position detection of the trapped beads.

#112464 - $15.00 USD Received 10 Jun 2009; revised 10 Jul 2009; accepted 11 Jul 2009; published 23 Jul 2009

The close-up of the optical trap is shown in Fig. 2(b). Two lensed fiber were attached to a board via two 3D translation stages (3D Stages 1 and 2) to facilitate fiber alignment, which was achieved by examining the positions of the optical beams at different focal planes. Due to the scattering, the auras of the optical beams can be seen from the microscope images (see Fig. 3). When the objective moves along the z axis, the aura of each beam will move along a line parallel to the y axis. The x-axis fiber alignment was achieved when both auras moved along a common line, while the z-axis alignment was realized when the distances between the auras and the corresponding fiber tips were the same. After the fiber alignment was achieved, Stages 1 and 2 were fixed so that the board containing the two fibers can be moved as a whole block by adjusting a common stage (3D Stage 3). The optical beam emitted from the lensed fiber has a waist radius of 1.35±0.25 μm, which is located 12±2 μm from the end face of the fiber, according to the data provided by the manufacture. The fibers are arranged with an inclination angle $\theta = 50^{\circ}$. This inclination angle can be changed to investigate the influence on the trapping performance. The separation between the two fibers is 45 μm along the y axis. It is noted that the beam intersection is located around 17 μm downstream below the beam focuses, rather than at the focuses where a stronger trap can be achieved. This is due to the limitation of the fiber tip geometry, which has a cone shape with an opening angle of around 90 degrees, as shown in Fig. 1(b). If the fibers are arranged so that the beam intersection (where the trap is) is at the two focuses, the fiber tip geometry will prevent the intersection from reaching the substrate, and hence beads lying on the substrate cannot be picked up. A coverglass with a water drop containing silica beads (Bangs Laboratories, Inc.) is placed on a two-dimensional stage, which is attached to a one-dimensional motorized stage (UTM50MVTP, Newport Corp.) to achieve a constant moving speed for calibration purpose.

Silica beads of four different sizes from 3.01 to 4.74 μm in diameter were trapped in the experiment. The silica beads have a density of 2.0 g/cm^3 and a refractive index of 1.45 according to the data provided by the manufacturer. Beads solution was first diluted with distilled water by 600 times. To reverse bead aggregation, a glass beaker containing the diluted bead solution was immersed in ultrasonic bath for 15 minutes. One drop of the bead solution was then added on the coverglass, where the trapping experiment was carried out. The thickness of the water drop was controlled to be 3~4 mm. To prevent the water on the coverglass from drying up under the illumination light, water was added to the coverglass frequently.

3.2 Three-dimensional trapping ability

To demonstrate the 3D trapping ability, a silica bead in water was manipulated in three dimensions using the inclined DFOTs, as shown in Fig. 3. The two black shadows in the pictures were the fiber tips. The bead (Bead 1) that initially lay on the coverglass was trapped and then lifted by raising the trap. It is noted that the focal plane of the observing objective was fixed and all the pictures in Fig. 3 were captured on the same vertical plane while the trap or the water were moved. When Bead 1 was trapped, the coverglass can be moved freely along the x or y direction (Fig. 3(b)-3(f)), and another bead (Bead 3 in Fig. 3(f)-3(h)) can move below Bead 1 without any interference.

3.3 Calibration of trapping efficiency with drag force method

In order to use the inclined DFOTs for force sensing, the trapping efficiency and the spring constant must be calibrated. The drag force method [1] was used to obtain the calibration results below. After trapped, the bead was lifted to at least 50 μm (about 10 times the bead diameter) above the substrate in order to reduce side wall effects in drag force calculation. To measure the bead displacement, a video was captured with the CCD video camera from the beginning of the motion. The bead displacement at each frame was obtained by performing image correlation. A mean value of displacement after the bead reached equilibrium was

#112464 - $15.00 USD Received 10 Jun 2009; revised 10 Jul 2009; accepted 11 Jul 2009; published 23 Jul 2009

consequently obtained as the equilibrium position, which depends on the water speed. The optical force exerted on the bead was calculated by the drag force, which can be expressed as [23]

$$F_{drag,bead} = 6\pi\mu v r, \tag{1}$$

where μ is the viscosity (8.9×10^{-4} Pa·s for water), v is the speed of the water (along the x axis), and r is the radius of the bead. By varying the water speed, the dependence of optical forces on displacements of the trapped bead was obtained.

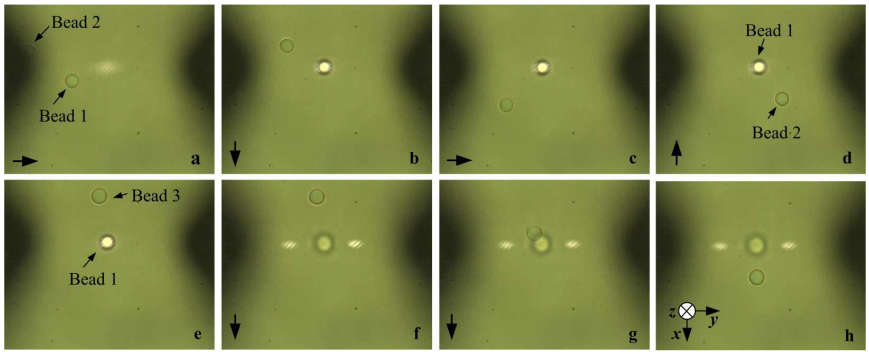

Fig. 3. Silica bead with a diameter of 4.74 μm being manipulated in three dimensions by the DFOTs. The arrows indicate the next motion direction of the coverglass. (a) Initial positions of free beads with the coverglass moving along +y. (b)-(c) The coverglass moving along +x with Bead 1 trapped. (c)-(e) The coverglass moving along +y, -x, and then -y. Bead 2 was moved out of the view field and another free bead, Bead 3, was brought in. (e)-(f) The trap together with Bead 1 moving out of focus along +z. (f)-(h) The coverglass moving downwards (+x) with Bead 3 moving freely below Bead 1. (Media 1) 2.7 MB.

In order to ensure that the measurement of bead displacement was faithful, the fiber tip deflection due to the drag force needs to be estimated. According to the equation derived by Lamb [25], when the Reynolds number is small compared to 1, the drag exerted on a cylinder that has only translational motion in the water with its axis perpendicular to the flow direction can be expressed as

$$F_{drag,cyl} = \frac{4\pi\mu v l_c}{0.5 - \gamma - \ln(\frac{\rho v D}{4\mu})}, \tag{2}$$

where l_c is the length of the cylinder, γ is the Euler-Mascheroni constant (~0.577), ρ is the density of water, and D is the diameter of the cylinder. For the optical fiber, D = 125 μm, rendering a Reynolds number of 0.073. The maximum flow speed of 80 μm/s and the fiber immersion length of 10 mm are used to calculate the fiber tip deflection. Based on Eq. (2), the drag force exerted on the fiber can be obtained ($F_{drag,cyl}$ = 1540 pN). If the fiber is considered as a clamped pure silica (Young's modulus of 46 GPa [26]) cylinder with a suspension length of 15 mm, and it is subject to a concentrated load ($F_{drag,cyl}$) at the free tip, a deflection of 0.19 nm at the free tip can be obtained. It is noted that all the parameters have been chosen to ensure a safe estimation. Since this estimated fiber tip deflection is three orders of magnitude smaller than the bead displacement (in sub-micrometers), it is safe to neglect the fiber tip deflection due to the drag of the flow.

To compare the optical forces obtained with respect to different optical powers, trapping efficiencies were calculated, which describes the transfer efficiency from the momentum of the light to that of the trapped object. The trapping efficiency is defined as [24]

#112464 - $15.00 USD Received 10 Jun 2009; revised 10 Jul 2009; accepted 11 Jul 2009; published 23 Jul 2009

$$Q = \frac{Fc}{nP}, \tag{3}$$

where F is the optical force, c is the speed of light in vacuum, P is the optical power, and n is the refractive index of the medium (in our case, n = 1.33 for water). The experimentally obtained trapping efficiencies at different optical powers are shown in Fig. 4. Every single data point is the mean value of the displacements obtained from video clips with duration of at least 5 seconds.

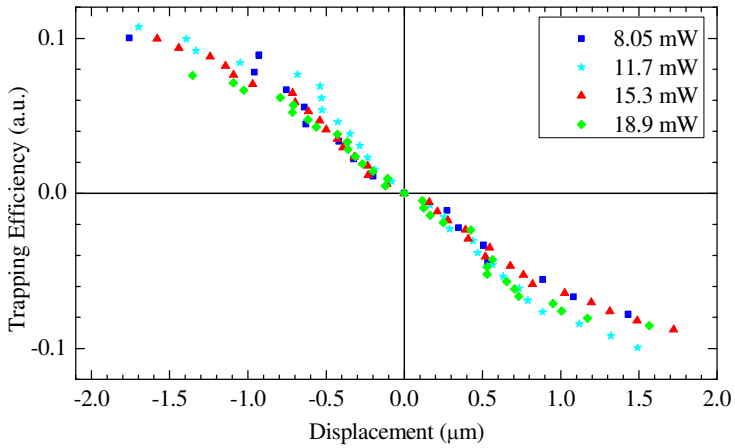

Fig. 4. Calibration curves of x-axis trapping efficiencies obtained with different laser powers. The experiments were carried out with silica beads of 4.74 μm in diameter. The optical powers shown are the total powers from both fibers.

According to the calibration results shown in Fig. 4, the trapping efficiency is linearly dependent on the displacement within the range of −1 μm to +1 μm, which bestows the DFOTs an ability to carry out force sensing. Moreover, the superposition of the trapping efficiencies at different optical powers implies that the trapping efficiency does not depend on the optical power, which is intuitive and can be explained by its definition.

3.4 Calibration of trapping efficiency with power spectrum analysis

In addition to the drag force calibration, power spectrum analysis method [1, 27] was used to obtain both the x- and y-axis spring constants. We chose this method because the power spectrum of trapped beads can also be used to diagnose possible problems of the optical tweezers, such as alignment errors and other system noise, which cannot be provided by other calibration techniques such as the equipartition method. [1] The power spectrum (P_x) of the PSD output voltage due to the Brownian motion of the trapped bead in the x direction is a Lorentzian function of the frequency f [27]:

$$P_x = \frac{D/2\pi}{f^2 + f_c^2}, \tag{4}$$

where the constant D and the corner frequency f_c are two parameters obtained from curve fitting. The x-axis spring constant can be calculated by

$$k_x = 12\pi\mu r f_c. \tag{5}$$

Identical equations apply to the y axis. In our experiments, the power spectra were obtained by collecting the light scattered by the trapped bead using the PSD. In order to minimize the sidewall effect, the beads were trapped in three dimensions and then lifted up to around 35 μm

#112464 - $15.00 USD Received 10 Jun 2009; revised 10 Jul 2009; accepted 11 Jul 2009; published 23 Jul 2009

above the coverglass. The PSD output data were collected within a time period of 50 seconds at a sampling frequency of 10 kHz. This sampling frequency is much larger than the measured corner frequencies (less than 20 Hz) so that faithful results can be obtained. The power spectra were blocked before the curve fitting by replacing 100 consecutive data points with the averaged data point at the corresponding mean frequency. This is necessary because the power spectra obtained from the experiment are exponentially distributed. After data averaging with a sufficient large number of blocking points, the power spectra approaches Gaussian distribution and the least-squares fitting can be used [27]. Curve fitting of the experiment data with Eq. (4) was carried out within the frequency range from 1 Hz to 2 kHz. The spring constants were calculated from the fitted corner frequency f_c according to Eq. (5). As an example, a fitted x-axis power spectrum obtained with a bead size of 4.74 μm and the optical power of 18.9 mW is shown in Fig. 5. The spring constant obtained from the power spectrum analysis (2.82 pN/μm) compares well with that obtained from the drag force calibration at the same power (2.98 pN/μm).

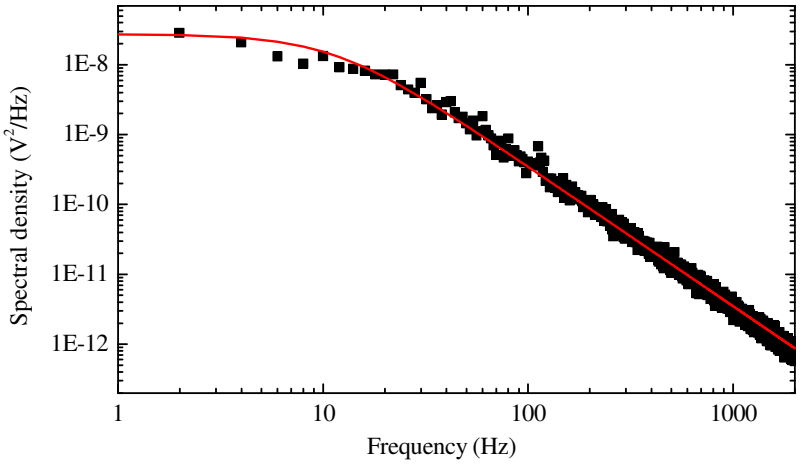

Fig. 5. Lorentzian fitting (red curve) of experimentally measured power spectrum (black squares). Here, the corner frequency f_x is 11.3 Hz, which gives a spring constant k_x of 2.82 pN/μm.

It is noted that the trapped bead was not imaged onto the PSD plane. Since the trapped bead was close to the two laser beams but off-axis, not all the optical power was scattered. If the bead center were conjugate to the PSD plane, the scattered light could be overwhelmed by the unscattered light, and Lorentzian fitting of the experimental data could fail. To solve this problem, the objective was lowered by a proper distance so that the images of the two optical axes were further away from the bead center, resulting in less unscattered light registered at the PSD. However, the objective could not be lowered too much. Otherwise, the scattered light collected by the PSD was not strong enough and a good fitting could not be achieved, either. In our experiments, the proper distance to lower the objective was found to be within 50 μm to 75 μm in order to minimize the influence of the unscattered light. Since the optical axes were located in the yz plane, y-axis power spectra were influenced more than x-axis power spectra.

Both x- and y- axis spring constants of four different bead sizes were calibrated under the power of 18.9 mW. The results are summarized in Table 1. It can be seen that the larger the bead, the higher the spring constants. The x-axis spring constants were always larger than the y-axis spring constants. This is intuitive since no scattering forces appear along the x axis while along the y axis, the scattering forces prevent the bead from being trapped (see Fig. 1(b)).

#112464 - $15.00 USD Received 10 Jun 2009; revised 10 Jul 2009; accepted 11 Jul 2009; published 23 Jul 2009

The calibration results along with the experimental results obtained in Section 3.2 demonstrate that the inclined DFOTs can serve as both a 3D actuator that is able to pick up particles lying on the substrate and a force sensor. By detecting the displacement of the trapped particle, the external forces applied on the particle can be measured.

Table 1. Spring constants of different bead sizes.

Bead diameter (μm)	Experiment		Simulations	
	k_x (pN/μm)	k_y (pN/μm)	k_x (pN/μm)	k_y (pN/μm)
4.74	2.82	1.86	2.35	1.01
3.93	1.71	1.16	1.64	0.66
3.50	1.38	0.74	1.05	0.43
3.01	1.21	0.34	0.70	0.17

3.5 Influence of the fiber inclined angle θ

In addition to the influence of the optical power, the trapping performance with respect to different fiber inclination angles θ is also investigated. At the total power of 8.05 mW, θ was decreased with an increment of 5° while keeping the same fiber distance. The reason to choose this optical power is that the trap was the weakest amongst the four powers that were used in the experiments. When the trap is weaker, it is more sensitive to the influences of the parameters including θ, and thus the consequence of changing parameters becomes easier to observe.

The beads could not be lifted up when $\theta \leq 45°$ in the experiments, but they can still be trapped in two dimensions along the x and y directions. For $\theta \geq 50°$, the bead can be lifted up, and thus trapped in three dimensions. Given the same optical power, the DFOTs exhibit a stronger z-direction trap for a larger θ value. These results imply that the trapping performance along the z direction also depends on the inclination angle. The 3D trapping degrades into a 2D trapping when the inclination angle is below a critical value, which was obtained to be between 45° and 50° in the experiments.

4. Simulations

4.1 Model

It is assumed in our simulations that the optical beam emitted from the lensed fiber has a Gaussian profile (i.e., operating on the fundamental transverse mode (TEM_{00} mode)) and the beam is unpolarized. When the particle size is in Mie regime, the forces exerted on the particle can be derived based on a ray-optics model including the Gaussian beam profile. [28, 29] Generally ray-optics is a good approximation when the particle size is 10 times larger than the wavelength. In our simulations, since the particle size is 3.7~5.9 times larger than the wavelength, this requirement is not completely fulfilled. However, the simulations can still provide reasonable results when the wavefront curvature of the incident beam is incorporated into the ray-optics model. [28] To calculate the optical force exerted by a Gaussian beam, the surface of the trapped object is divided into finite number of small surface fractions. The direction and the intensity of the ray that shines on each surface fraction can be determined according to the Gaussian beam profile. The optical force component on each surface fraction can be obtained by calculating the difference between the photon momentum that the incident ray brings in and that the refraction and reflection ray take away. The total optical force exerted on the object is then calculated by adding up all the optical force components over the

#112464 - $15.00 USD Received 10 Jun 2009; revised 10 Jul 2009; accepted 11 Jul 2009; published 23 Jul 2009

entire object surface. The trapping force of the DFOTs is obtained as the sum of the optical force vectors applied by both optical beams emitted from the two fibers.

The coordinate system used in the simulations is shown in Fig. 1(b). In order to compare the simulation results with the experimental results, the parameters (the wavelength, the focus size, the distance between the fibers, the fiber inclination angle, the bead size and refractive index) are selected to be the same as those used in the experiments except for the parameter (the fiber inclination angle or the bead size) that is changed to investigate the influence to the trapping performance.

4.2 Trapping force in the z direction

Since the main difference between the SFOTs and the DFOTs is the z-axis trapping ability, the optical force obtained with the DFOTs along the z-axis is studied first. The z-axis optical force as a function of the bead displacement along the z axis is shown in Fig. 6 when the total optical power is 8.05 mW. The origin of the displacement is at the beam intersection. The results obtained with different fiber inclination angles are compared here.

In order to lift up the bead, the optical force should be larger than the gravity minus buoyancy (G-F_b), which is illustrated as the horizontal dashed line in Fig. 6. It can be seen that levitation can only be realized when $\theta \geq 50°$. Larger θ values provide a higher $+z$ optical force, and hence a stronger z-axis trap. In the case when $\theta \leq 45°$, the DFOTs fail to lift up the bead along $+z$ direction. This defines a critical angle θ between 45° and 50° for levitation, which matches the value observed in the experiments.

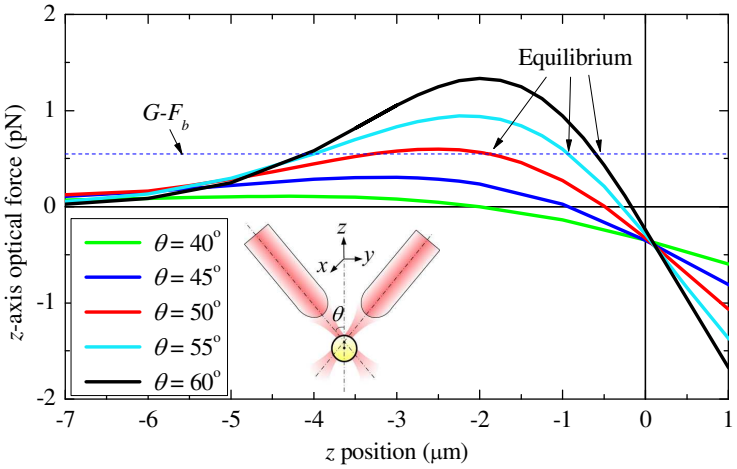

Fig. 6. The simulation results of optical force versus bead displacement along z axis with different θ values. G is the gravity and F_b is the buoyancy of the trapped silica bead. The optical force should be larger than G-F_b in order to trap the bead in the z direction. The figure implies that 50° is the critical angle for z-axis trapping, which coincides with the experimentally observed value. The total optical power emitted from both fibers is 8.05 mW. The bead size is 4.74 μm in diameter.

It is noted that the equilibrium position of the trapped bead is not at the beam intersection but somewhere below the intersection and that it varies with respect to the value of θ and the optical power. The equilibrium position can be obtained from Fig. 6 as the right intersection (where a restoring force exists) of the optical force curve and the G-F_b line. For example, for a given θ of 50°, the equilibrium position is 1.88 μm below the beam intersection when the optical power is 8.05 mW, while the value changes to 1.03 μm at the power of 15.3 mW. This is intuitive because a lower power renders a lower optical force at the same position. Therefore, if the power decreases, the trapped bead will be trapped downwards away from the

#112464 - $15.00 USD Received 10 Jun 2009; revised 10 Jul 2009; accepted 11 Jul 2009; published 23 Jul 2009

optical beams so that the optical force can be increased to reach the value needed for a lift-up. When the power gets too low, the bead eventually escapes from the trap.

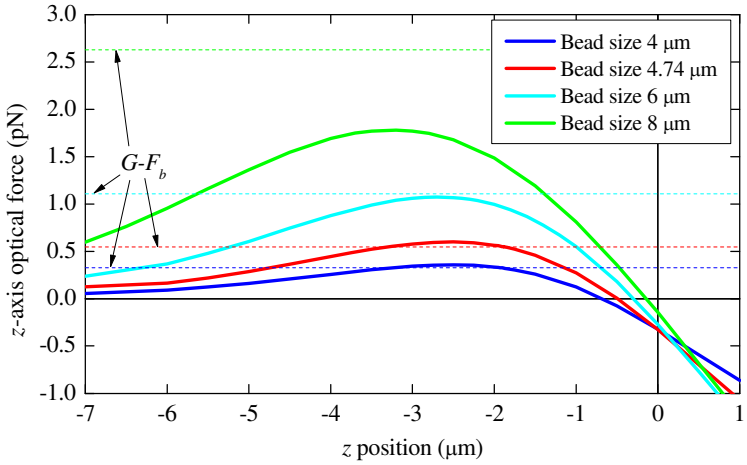

Fig. 7. The simulation results of optical force versus bead displacement along z axis with different bead sizes. G is the gravity and F_b is the buoyancy of the trapped silica bead. For each bead sizes, G-F_b is expressed with a horizontal dashed line with the same color as the optical force curve. The figure implies that large particles are more difficult to be lifted up. The total optical power emitted from both fibers is 8.05 mW. The inclination angle θ is 50º.

The influence of the bead size on the z-axis trapping ability is shown in Fig. 7. The red curve shows the results obtained with one of the bead sizes used in the experiments. It can be seen that larger particles are more difficult to lift up with the same DFOTs setup. At the optical power of 8.05 mW, beads with sizes equal or larger than 6 μm cannot be lifted up, whereas smaller beads with sizes of 4.74 μm and 4 μm can. Actually, the beads with the sizes between 3.01 μm and 4.74 μm were lifted up in our experiment. The reason can be explained as that the gravity of the bead increases more quickly with the increasing bead size than the optical force does. Therefore, in order to trap larger particles, either the optical power or the inclination angle needs to be increased.

4.3 Trapping forces along the x and y directions

The trapping forces versus the displacements along the x and y axes are shown in Fig. 8. The bead size of 4.74 μm and the optical power of 15.3 mW are used in order to compare with the experimental results. The influence of inclination angles to the x- and y-axis trapping forces is investigated. It is noted that the z coordinate is fixed to be −1.03 μm, −0.59 μm, −0.39 μm, −0.17 μm, and −0.10 μm for the curves with the inclination angle of 50º, 55º, 60º, 75º, and 90º, respectively. These values of the z coordinate correspond to the equilibrium positions of the bead located on the z axis, which are obtained by finding the intersections of the z-axis optical force curves with the horizontal G-F_b lines (data not shown). Here, only the cases when a 3D trapping is formed are studied, i.e., the inclination angles $\theta \geq 50º$.

According to the x-axis optical forces obtained from the DFOTs shown in Fig. 8(a), both the simulation and the experimental results exhibit the existence of a restoring force when the bead is displaced from the equilibrium. The slope of the x-axis optical force curves in the vicinity of the origin, or the spring constant, can be obtained with curve-fitting. The spring constant obtained from the experiments (2.68 pN/μm) and the simulations (1.90 pN/μm) are in the same order of magnitude. If the drag force keeps increasing from 0, the bead will be displaced from the trap until a maximum displacement is reached, which corresponds to the displacement at the peak or in the valley of the x-axis optical force curve obtained from the

#112464 - $15.00 USD Received 10 Jun 2009; revised 10 Jul 2009; accepted 11 Jul 2009; published 23 Jul 2009

simulations. A larger displacement cannot be obtained experimentally as the bead will escape from the trap. The maximum displacement obtained in the simulations (±2.0 μm) compares well with that observed in the experiment (−1.6 μm along –x and +1.7 μm along +x). The x-axis simulation results obtained with different fiber inclination angles (θ) implies that the larger the inclination angle θ, the larger the x-axis optical force (or the spring constant). This is because z-axis equilibrium position and beam waist position change with different inclination angle. For a larger θ, the bead is trapped to a position closer to the beam intersection, where the optical intensity is the highest. Furthermore, as the fiber separation is fixed, the beam waists are closer to the beam intersection for a larger inclination angle. Both factors contribute to the increase of the x-axis optical force when the fiber inclination angle increases.

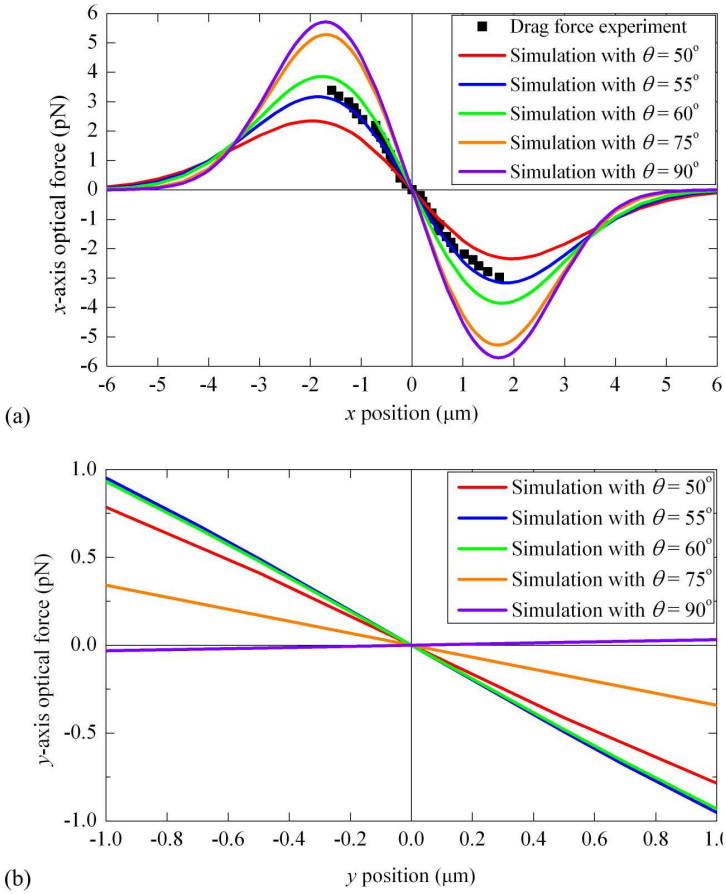

Fig. 8. The dependence of optical forces on bead displacements along (a) the x axis and (b) the y axis at different fiber inclination angles. The total optical power emitted from both fibers is 15.3 mW. The bead size is 4.74 μm in diameter. The fiber separation along the y axis is 45 μm.

The spring constant obtained from the drag force experiments is larger than that obtained from the simulations. The sources of errors include the error in the measurement of the fiber inclination angle θ, misalignment of the two fibers, and the beam profile being non-Gaussian and partially polarized. The error of θ measurement in the experiment was ±2°. According to the results shown in Fig. 8(a), the x-axis optical force with $\theta = 55°$ is 1.5 times larger than that with $\theta = 50°$. The error in the measurement of θ may result in the error between the simulation

#112464 - $15.00 USD Received 10 Jun 2009; revised 10 Jul 2009; accepted 11 Jul 2009; published 23 Jul 2009

and the experimental results. The alignment of the two fibers in the *xy* plane is realized under the microscope objective, which has a good accuracy (~ 1 μm). However, it is difficult to achieve exactly the same height along the *z* axis for the two fibers. In this case, the *z*-axis misalignment may result in errors of the simulation results, which are obtained when assuming no misalignment occurs. The polarization is also a possible source of errors, since the light emitted from the lensed tip might still be partially polarized.

The optical forces along the *y*-axis verses the *y*-axis displacements with different inclination angles are shown in Fig. 8(b). It should be noted that these curves are obtained at fixed, non-zero *z* coordinates, i.e., the bead motion is considered to be parallel to the *y* axis. This is only valid for small (in submicrons) *y* displacements. Since the two optical beams are located in the *yz* plane, the *y*-axis bead displacement is inevitably confined by the two optical beams. For example, at an inclination angle of 50°, the experimentally obtained *y*-axis displacement was within -1 μm and 1 μm in order to maintain a 3D trap. In this sense, *y*-axis trapping has a less displacement allowance, and hence is less stable compared with the *x*-axis trapping. However, it is worth emphasizing that, since the experimental calibration with the power spectrum method was carried out only for small *y* displacements, Fig. 8(b) does reflect the condition in the experiment. Therefore, the spring constants obtained from Fig. 8(b) are valid in the vicinity of $y = 0$ and can be used to compare with the experimental results. According to the results shown in Fig. 8(b), the *y*-axis optical force as well as the spring constant around the *z* axis first increases and then decreases as θ is increased from 50º to 90º. The maximum spring constant occurs when θ is around 60º. When $\theta = 90º$, the DFOTs becomes a counter-propagating configuration, and the spring constant is positive, which means the equilibrium on the *z* axis is no longer stable. This result agrees with the previous work of Sidick *et al.* [16], in which the center position in the counter-propagating DFOTs was found to be unstable when the beam waists were set to be close to each other.

The *x* and *y*-axis spring constants of different bead sizes (3.01 μm, 3.50 μm, 3.93 μm, and 4.74 μm) at the power of 18.9 mW were obtained from simulations. The results are included in Table 1. The simulation results are consistent with the experimental results obtained from power spectrum analysis, indicating that larger beads have larger spring constants. In addition to the fiber misalignments and errors in θ measurements discussed above, the influence of the unscattered light can also contribute to the differences between the experimental and the numerical results. Since the ray optics model can serves as a good approximation only when the bead size is much (>10 times) larger than the wavelength. The fact that the bead sizes are not much larger than the wavelength may also cause errors between the experimental and simulation results, especially for small bead sizes (3.01 μm and 3.50 μm).

4.4 Robustness of the DFOTs to z-axis misalignment

In a practical system setup, fiber misalignment is inevitable for both inclined DFOTs ($\theta < 90º$) and counter-propagating DFOTs ($\theta = 90º$). Since the *y*-axis misalignment corresponds to the variation of the fiber separation, only the misalignments along the *x* and *z* directions are of interest. If an *x*-axis misalignment exists, inclined DFOTs and the counter-propagating DFOTS will exhibit similar robustness to such misalignment. The tolerances of the two configurations to *z*-axis misalignments are important to investigate since it can help determine whether a 3D trapping capability can be maintained. In Fig. 9, the 2D force fields are obtained for both configurations when there exists a misalignment of 1 μm along the *z* direction (the right fiber is higher than the left fiber). For counter-propagating DFOTs, the misalignment of 1 μm is a practical value when the two fibers are embedded in the V-grooves of a substrate. [30] The misalignment may caused by the environmental influence on the adhesive and by the uncontrollable adhesive thickness between the fiber and the inclined walls of the V-groove. In the inclined DFOTs, the heights of the fiber tips along the *z* axis are measured based on the distance between each optical beam (the auras in Fig. 3) and the corresponding fiber tip along

#112464 - $15.00 USD Received 10 Jun 2009; revised 10 Jul 2009; accepted 11 Jul 2009; published 23 Jul 2009

the *y* axis. The precision level of 1 μm is readily achievable in our inclined DFOTs setup since the smallest feature size of the objective images is below 1 μm. In the simulations, each fiber is considered to emit a power of 7.65 mW, and the fiber separation is 45 μm along the *y* axis for both the inclined and the counter-propagating DFOTs.

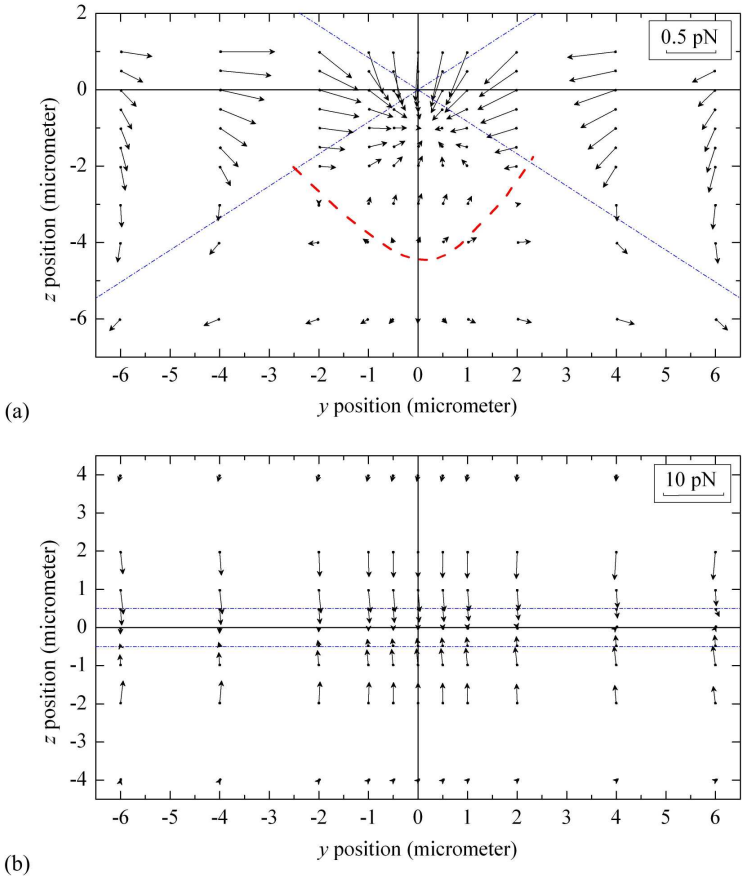

Fig. 9. Simulation results of the forces applied on a 4.74-μm bead in the *yz* plane with a misalignment of 1 μm along the *z* axis for (a) the inclined DFOTs ($\theta = 50°$) and (b) the counter propagation DFOTs ($\theta = 90°$). The blue dash-dotted lines indicate the optical axes of the two fibers. It is noted that the forces are the net forces of optical forces, gravity, and buoyancy applied on the beads.

Figure 9(a) shows the results obtained from the inclined DFOTs when $\theta = 50°$. The two beams still intersect despite of the existence of a *z*-axis misalignment. According to the force directions, it can be seen clearly that a 3D trap exists in the vicinity of the point (0, -1 μm). Moreover, the trap position moves to the right of the *z* axis instead of staying on the *z* axis when there is no misalignment. This is due to the asymmetry introduced by different beam waist positions with respect to the beam intersection. The beam waist of the left fiber is closer to the beam intersection, and hence can induce larger optical forces applied to the bead, if the bead is moving on the *z* axis. In order to balance this asymmetry, the bead moves closer to the beam emitted from the left fiber, which is to the right of the *z* axis. The red dashed curve in Fig. 9(a) defines the region where the bead will be trapped. If the bead is located above the red curve, it will be trapped in three dimensions. The optical force is not strong enough to lift up the bead if it is below the red curve. If the bead is to the right or the left of the red curve, it will be trapped by a single optical beam and be pushed downstream.

#112464 - $15.00 USD Received 10 Jun 2009; revised 10 Jul 2009; accepted 11 Jul 2009; published 23 Jul 2009

The results obtained from the counter-propagating DFOTs are shown in Fig. 9(b). The force field is "twisted" counter-clockwise in the vicinity of the origin, which means that there is no effective trapping region where all the surrounding forces are pointing inside. Instead of staying at the stable position, the bead will circle around the origin, if the bead is close (i.e., < 2 μm) to the origin. If the bead is far (i.e., > 4 μm) from the origin, SFOTs become dominant and the bead will be pushed away along the optical axis of one fiber.

By comparing the force fields of the two systems with respect to *z*-axis misalignment, it can be seen that, with the same fiber separation, the inclined DFOTs are more robust to the misalignment along the *z* direction. Although *z*-axis fiber misalignment in the inclined DFOTs influences the trapping efficiency as mentioned previously, its 3D trapping capability is retained. However, the counter-propagating DFOTs will lose the 3D trapping capability even with a 1-μm misalignment due to the twisted force field. When the *z*-axis misalignment increases, the twisting effect of the counter-propagating DFOTs becomes even worse and the trapping becomes more difficult. By contrast, simulation results (data not shown) show that the inclined DFOTs can still achieve a stable 3D trap with a *z*-axis misalignment of 8 μm.

When a much larger fiber separation or cleaved fibers instead of lensed fibers are used, the counter-propagating DFOTs suffer less from the *z*-axis misalignment (data not shown). In this sense, large (> 100 μm) fiber separations and cleaved fibers are preferable for the counter-propagating DFOTs to obtain stable trapping of particles. By contrast, for the inclined DFOTs, lensed fibers and smaller fiber separations are preferable to increase the trapping efficiency and to ensure the 3D trapping ability.

As for the limitations of the inclined DFOTs compared with the counter-propagation DFOTs, the inclined DFOTs have a longer fiber suspension length, and hence the stability of the trap is more susceptible to the movement of the fibers, which may be induced by the flow passing through the fibers. In addition, although the block containing two fibers (the board with two attached fibers in Fig. 2(b)) provides the inclined DFOTs flexibility, the complexity of the system is inevitably increased by introducing another surface for attaching the block besides the substrate. Therefore, the counter-propagating DFOTs are simpler and can provide stable traps if fibers are properly aligned, whereas the inclined DFOTs are more flexible and more robust to the fiber misalignment.

5. Conclusions

In this article, 3D trapping ability of the inclined DFOTs has been demonstrated and its trapping efficiency has been calibrated experimentally. The calibration enables the inclined DFOTs to serve as a force sensor. Parametric studies by means of numerical simulations have been carried out to better understand the system. The spring constants obtained from simulations and experiments along the *x* and *y* axes are in the same order of magnitude. It has been found that there is a critical value of the inclination angle, over which a 3D trap is enabled, and the value observed in experiment matches that obtained from the simulations. Moreover, the inclined DFOTs have been found to be more robust to the *z*-axis misalignment of the two fibers when compared with the counter-propagation DFOTs, although the latter is a special case of the former with the inclination angles of both fibers being 90º. The inclined DFOTs can find applications where a flexible and integratable 3D trapping method is needed, for example, lab-on-a-chip systems and microfluidic systems. In these systems, the inclined DFOTs can be attached to a microelectromechanical (MEMS) actuator to enable 3D manipulation and force sensing of biology specimens.

#112464 - $15.00 USD Received 10 Jun 2009; revised 10 Jul 2009; accepted 11 Jul 2009; published 23 Jul 2009